Available online at www.sciencedirect.com
ScienceDirect
Journal of Crystal Growth 308 (2007) 269–277
JOURNAL OF CRYSTAL GROWTH
www.elsevier.com/locate/jcrysgro

Selective silicon nanoparticle growth on high-density arrays of silicon nitride

Shawn S. Coffee[a], Davood Shahrjerdi[b], Sanjay K. Banerjee[b], John G. Ekerdt[a,*]

[a]*Department of Chemical Engineering, University of Texas at Austin, Austin, TX 78712, USA*
[b]*Electrical and Computer Engineering, University of Texas at Austin, Austin, TX 78712, USA*

Received 12 March 2007; received in revised form 13 July 2007; accepted 23 August 2007
Communicated by T.F. Kuech
Available online 2 September 2007

Abstract

Selective silicon nanoparticle deposition from disilane on ~17 nm diameter Si_3N_4 features defined through a 15-nm-thick SiO_2 masking layer was studied using hot wire chemical vapor deposition between 900 and 1025 K, and chemical vapor deposition between 900 and 975 K. Thin film poly(styrene-b-methyl methacrylate) diblock copolymer was used to generate cylinders with a density of $6 \times 10^{10}\,cm^{-2}$ that served as the patterning template. Silicon adatom etching of SiO_2 and diffusion of adatoms to the Si_3N_4 regions prevented the accumulation of adatoms necessary for nanoparticle nucleation and growth on the SiO_2 surfaces. Nanoparticles form selectively on Si_3N_4, because adsorbed Si does not etch this surface. Incident flux, total exposure, and substrate temperature were adjusted to explore nanoparticle deposition trends relating relative adatom concentration with nanoparticle density and size distributions.

PACS: 81.15.Gh; 81.05.Gy; 81.16.Nd; 83.80.Uv; 81.07.−b

Keywords: A1. Nanoparticles; A3. Chemical vapor deposition; B1. Nitrides; B1. Oxides; B1. Silicon

1. Introduction

Since the beginning of the integrated circuit industry in the 1960s, device performance has increased significantly as device dimensions decreased. With current devices being fabricated on the nanometer scale, final products magnify fabrication errors as the tolerance magnitudes decrease. Silicon nanocrystal-based flash memory has been successfully fabricated and tested as a proposed future generation device using nanocrystals grown via chemical vapor deposition (CVD) [1,2]. As the size of the memory cell decreases in the future [3], reliable device operation demands a low particle size distribution and ordered lateral placement. CVD nucleation on amorphous insulator surfaces is unorganized in nature due to randomly positioned nucleation sites [4–6], and spatially restricting the domain region over which nucleation occurs is one approach toward ordered lateral nanoparticle placement.

We have previously shown with Ge [7] that selective nanoparticle placement is possible during hot wire chemical vapor deposition (HWCVD) by employing a thin (12 nm) SiO_2 mask through which ~22 nm vias are etched to expose HfO_2. The more facile etching by adsorbed Ge of SiO_2 versus HfO_2 [8] affords a kinetic window between 700 and 800 K in which the Ge adatoms can accumulate on HfO_2 and not on SiO_2, and eventually nucleate and grow into nanoparticles selectively on the HfO_2 regions. The lower limit of this window is set by a temperature required to etch SiO_2 faster than the adsorption of Ge (or more correctly GeH_x by thermally cracking GeH_4 over a filament). The upper temperature is set to minimize Ge loss from HfO_2 by etching reactions. The kinetic window for Si etching of SiO_2 versus HfO_2 is more narrow (900–925 K), and as a consequence Si nanoparticle growth is not as selective as was found for Ge. Silicon nanoparticles deposited at 900 K were found on both SiO_2 and

*Corresponding author. Tel.: +1 512 471 4689; fax: +1 512 471 7060.
E-mail address: ekerdt@che.utexas.edu (J.G. Ekerdt).

0022-0248/$ - see front matter © 2007 Elsevier B.V. All rights reserved.
doi:10.1016/j.jcrysgro.2007.08.024

HfO_2, however, with a considerably higher density on HfO_2 [9]. Silicon nitride is not etched by adsorbed Si [10] and is therefore ideally suited for the selective CVD growth of Si nanoparticles employing a SiO_2 sacrificial mask. With Si on Si_3N_4 there is no upper etching limit, enabling one to work over a wider temperature range to observe the effects of adatom concentration on nucleation and growth.

The kinetics of Si and Ge island nucleation and nanoparticle growth have been reported on SiO_2 and Si_3N_4 surfaces [10–13]. Modeling approaches that relate island (or particle) density to the growth rate and temperature permit one to establish the critical cluster size, i^*, and the diffusion barrier for adatoms on the surface [14–17]. When one more adatom attaches to a critical cluster, a stable island/particle forms and beyond this i^*+1 condition the nucleated island/particle experiences growth. A critical cluster size of zero has been found for Ge on SiO_2 [11] and a value of 1 was assumed for Si on SiO_2 [13]. This implies that high adatom concentrations should not be required for nucleation on amorphous surfaces given that the density of unstable island/particles of size i that can grow into a critical cluster is proportional to the total adatom density to the power i, and the nucleation rate is proportional to the average adatom density to the power i^*+1 [16]. Activation energies of 0.13 eV [18] and 0.47 eV [13] have been reported for the diffusion of Ge on SiO_2 and Si on SiO_2, respectively, so the adatoms are expected to diffuse rapidly on the surface. The critical cluster size and diffusion energy are not reported for Si on Si_3N_4, however, they are likely to be similar in magnitude to those reported for Si on SiO_2.

Baron et al. [12] measured the total accumulation of Si into nanoparticles and referred to the accumulation rate as a nucleation-growth rate; they reasoned nucleation contributes most to the growth rate. They report nucleation-growth activation energies of 3.84 and 2.83 eV on SiO_2 and Si_3N_4, respectively [12]. Miyazaki et al. [4] reported that the activation energy for Si nanoparticle growth on thermally grown SiO_2 decreases from 4.8 to 1.75 eV by fully hydroxylating the surface through an HF etch and associated the lowered energy with a more reactive surface. Leach et al. [10] observed higher densities and attainment of these densities faster, or at lower temperatures, over Si_3N_4 versus SiO_2 and associated this to a more reactive Si_3N_4 surface toward activation of the Si_2H_6 precursor and with the complete retention of any Si adatoms on Si_3N_4. Even if the diffusion rates for Si on SiO_2 and Si_3N_4 are similar in magnitude, the diffusion is likely slower on Si_3N_4 and this would also contribute to a higher nucleation rate and density on Si_3N_4. Growth rates on SiO_2 and Si_3N_4 from hydride sources then appear to be controlled by the activation of the hydrides and their transformation into adatoms.

This paper reports the influence of adatom concentration on nanoparticle nucleation and growth within the confined regions. Due to the limited area, particles may occupy and the limited surface area on which Si adatoms can accumulate, the balance between adatom accumulation and Si loss through etching at the SiO_2 sidewalls is extremely sensitive to precursor flux and temperature. This balance affects formation of multiple particles growing within the pores and the fraction of pores with particles. CVD and HWCVD are employed to deliver either Si_2H_6 or SiH_x radicals to the surface.

2. Experimental procedure

Freescale Inc. provided the 15 nm plasma enhanced CVD SiO_2/30 nm plasma enhanced CVD Si_3N_4 grown stack structures 8 in p-doped Si(1 0 0) wafers. After dicing into smaller pieces, $3.2\times3.2\,cm^2$ sized portions were cleaned with an acetone/ethanol/deionized (DI) water rinse and then dried with compressed nitrogen. Patterning with a self-assembled diblock copolymer followed published schemes [19,20]. The exposed silica surface was initially pretreated with an α-hydroxy functionalized random copolymer (60% styrene and 40% methyl methacrylate, $M_n = 8900$ from Polymer Source Inc.) diluted 1% in toluene by spin coating at 1000 rpm for 30 s. The samples were annealed at 180 °C for 48 h allowing the –OH terminated end groups to react with the silica surface. Loose polymer strands were removed from the treated surface with a gentle toluene rinse followed by drying with compressed nitrogen. Poly(styrene-b-methyl methacrylate), $M_n = 46{,}100$ and 21,000 of styrene and methyl methacrylate species, respectively (Polymer Source Inc.), was diluted 1.1% in anisole and was spin coated onto the treated surface under conditions that produce a 37 ± 4 nm thick film that is critical for cylinder self-assembly normal to the substrate. This polymer formulation generates 20 nm diameter cylinders. Further annealing at 180 °C for 4 h caused the immiscible polymers to self-assemble. The minority methyl methacrylate cylinder phase was then selectively removed using a 5 min glacial acetic acid bath and a DI water rinse.

Pattern transfer through the 15 nm SiO_2 film used a CHF_3/O_2 reactive ion etch (RIE) at 200 W and 15 mTorr at room temperature. Silicon nitride is etched at less than half the rate of silicon dioxide under these conditions [21]. The time necessary to etch the SiO_2 was determined using a liftoff technique [19] in which incomplete Pd/Au films were sputtered on the RIE-etched samples before dipping in 1% HF to remove all remaining SiO_2. SiO_2 etches at a significantly higher rate in HF than silicon nitride, therefore, some sputtered metal remains behind after the HF etch, when the Si_3N_4 surface is reached during the RIE. As a check, the N 1s X-ray photoelectron spectroscopy (XPS) peak centered at 398 eV for silicon nitride was monitored in *ex situ* studies and it increases significantly as the nitride surface is exposed, signaling etch completion. The fully etched samples were then subjected to a 2s 1% HF etch to remove any residual SiO_2 from the bottom of the features. The final exposed silicon nitride pore diameter after

processing was 17 ± 3.2 nm with a pore density of 6×10^{10} cm^{-2}.

The etched samples were further diced into 1.6×1.6 cm^2 then loaded into an ultra-high-vacuum (UHV) CVD system [10] and annealed for 15 min at 1075 K to degas the surface and remove any potential SiO_xN_y native oxides [22] from the Si_3N_4 surface. This annealing step was necessary because Si etches the native oxide and this prevents Si adatom accumulation and Si nanoparticle nucleation during the early stages of a HWCVD experiment. *In situ* XPS confirmed removal of native surface oxides. Trace amounts of carbon were observed with XPS on the samples after annealing. The temperature was lowered to 975 K before Si_2H_6 (diluted 4% in He, from Voltaix Inc.) with a partial pressure of 2.0×10^{-8} Torr was admitted to the deposition chamber. The sample was placed ~3 cm from a tungsten cracking filament supplied with 4 A current (>1500 °C) resulting in a flux of 0.3 monolayer (ML)/min ($1\,ML = 6.8 \times 10^{14}$ atoms cm^{-2}). HWCVD occurs when Si_2H_6 molecules decompose on the hot filament with radicals desorbing and depositing on the heated sample surface. Fluxes were calibrated on thermally grown SiO_2 at room temperature by depositing an amorphous Si film [23]. XPS peak attenuation for the Si 2p peak of the oxide at 103.5 eV was used to establish the Si film thickness.

HWCVD studies explored total exposures equivalent to 1–15 ML, fluxes ranging from 0.1 to 0.9 ML/min, and temperatures ranging from 900 to 1025 K. CVD was conducted over a temperature range of 900–975 K while holding the disilane partial pressure at 1×10^{-4} Torr. Si deposition was confirmed *in situ* with XPS using Al K_α radiation. The Si 2p, O 1s, and N 1s peak binding energies were adjusted for charging using the C 1s peak (from trace contaminants) at 285 eV. The high-temperature process causes the silica hard mask to buckle locally in approximately 20% of the patterned samples, destroying small (~1000 nm^2 area) regions. One sample was given the 1075 K anneal without any silicon deposition and the buckling occurred revealing the initial anneal as the damage source. The buckled regions are not included within the particle statistics in this paper.

Upon removal from the system, the samples were coated with ~10 nm of Pd/Au to prevent surface charging under analysis in a Hitachi S-4500 field emission scanning electron microscope (SEM). Sputter coating onto blanket wafers was confirmed not to create features that could be interpreted as nanoparticles. Particle size and particle densities are determined by counting particles after digitally magnifying the SEM images. Nanoparticles less than ~5 nm in diameter are difficult to resolve. The particles were categorized with three designations according to diameter: small (5–8 nm), medium (9–11 nm), and large (13 nm and greater). When the entire pore is filled, a fourth category, film with a diameter of 17 nm, is used. For a given growth condition (sample), approximately 400 particles and never fewer than 300 particles were counted. The particle counts in each category are averaged to give an overall nanoparticle diameter. Particle crystallinity was not determined.

3. Results

It is possible to deposit Si selectively on Si_3N_4 and not on SiO_2 provided the etching rate of SiO_2 by adsorbed Si exceeds the rate of Si adatom generation. The SiO_2 etching reaction has an onset in TPD studies near 825 K and a peak maximum near 900 K [10]; therefore, the majority of the experiments reported herein were done at 975 K to ensure a rapid etching reaction under a continuous incidence of the silicon precursor. In addition, Si nanoparticles were not observed in SEM images on the SiO_2 surface for any samples.

Control experiments were preformed to determine if thermal CVD was possible on Si_3N_4 from Si_2H_6 at the HWCVD pressure of 2.0×10^{-8} Torr and with the cracking filament turned off. Fig. 1 presents the Si 2p peaks before and after exposure of extended Si_3N_4 to 2.0×10^{-8} Torr Si_2H_6 for 50 min with the cracking filament off. This particular pressure and time produces a 0.3 ML/min flux and 15 ML total deposition when the cracking filament is on. Slight variations in repositioning of the samples for XPS analysis makes comparison of absolute peak intensities an unreliable measure of changes in coverage when the peak differences are on the order of 10%, as reflected in the 102 eV feature for both 900 and 975 K. The ratio of the Si 2p XPS feature for metallic Si (99 eV) to the Si in Si_3N_4 (102 eV) should increase after CVD exposure when compared to the ratio before CVD exposure if Si is depositing on the Si_3N_4. This ratio increased from 0.099 before exposure to 0.123 after exposure at 900 K, an increase of 23%. The ratio increase was 29% at 975 K and 31% at 1025 K indicating that more Si was deposited at the higher temperatures. The SEM images (not shown) were featureless and this would result if any particles formed and were less than 3 nm in diameter. Therefore, we conclude that the Si_3N_4 surface is reactive enough that some level of Si adatom accumulation is possible from the uncracked Si_2H_6 that will also be present during the HWCVD experiments.

Studies have shown that defects can increase the nucleation density of Si nanoparticles on SiO_2 surfaces [24,25], so control experiments were performed to determine if the CHF_3/O_2 pattern transfer RIE process altered the reactivity of the Si_3N_4 at the bottom of the features. Fig. 2 presents SEM images for unpatterned, extended Si_3N_4 surfaces that had the SiO_2 layer removed by HF wet etching versus removed by the RIE process, followed by the brief (2s) 1% HF etch. These surfaces were subjected to Si CVD (1×10^{-4} Torr Si_2H_6) at 925 K for 4 min. The RIE-exposed sample reveals 5–25 nm Si nanoparticles with a density of 1×10^{11} cm^{-2}, while the HF-exposed sample had significantly less growth with 5–10 nm particles and a 2×10^{10} cm^{-2} density. Therefore the results for Si grown on

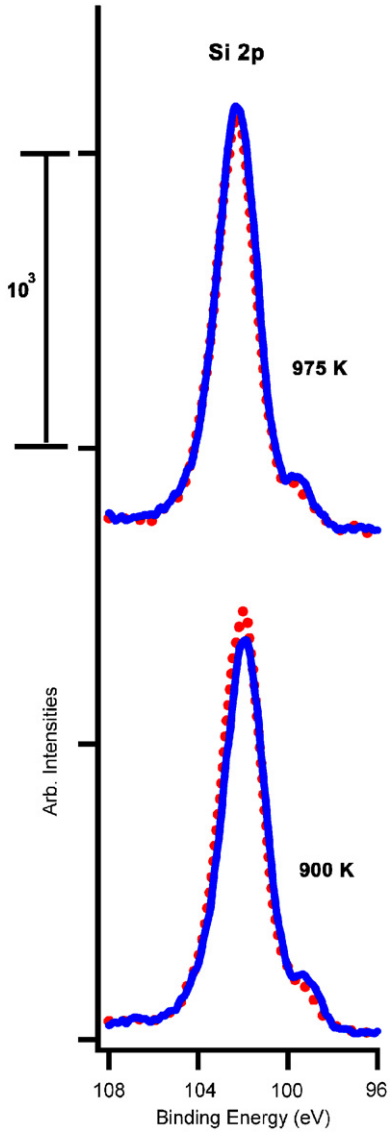

Fig. 1. XPS showing Si 2p signals for thermal CVD at 900 and 975 K. The 2.0×10^{-8} Torr Si_2H_6 partial pressure is equivalent to the background pressure used during the 0.3 ML/min HWCVD flux depositions. CVD exposure lasted 50 min or the equivalent amount of time required for a 15 ML HWCVD exposure originating at the tungsten filament generating radicals. (The dashed lines represent the signals before deposition.)

patterned Si_3N_4 regions in this study may not be directly correlated against those on as-grown Si_3N_4 extended surfaces because of the RIE process-induced damage. The nature of the defects and the cause for the increased nucleation were beyond the scope of this study.

Growth was observed in ~100% of the pores following 3 min of thermal CVD (18,000 Langmuir Si_2H_6) at all temperatures in the 900–975 K range. Silicon growth characteristics varied significantly with temperature. At 900 K, Si films that completely filled the pores formed and appeared to grow out of the pores and over portions of the SiO_2 mask since the Si 2p XPS feature associated with SiO_2 (103.5 eV) was attenuated. The fraction of pores that were filled by a complete film decreased with increasing temperature as illustrated in Fig. 3. As the temperature increased, the average diameter of the Si deposited decreased, reaching 11 nm at 975 K. Counting a continuous film as one particle, the density increased from the pore density value of $6.0 \times 10^{10}\,cm^{-2}$ at 900 K to 6.1×10^{10} and $6.7 \times 10^{10}\,cm^{-2}$ at 950 and 975 K, respectively. The changes in size and density, with temperature suggest less coalescence of particles, is occurring because less growth is taking place. Two factors can contribute to a lower growth rate with increasing temperature; an increase in Si loss through etching of SiO_2 at the pore perimeter and a decreasing sticking probability for the hydride precursor [26,27].

HWCVD can circumvent the decreasing sticking coefficient in that SiH_x radicals formed on the heated filament are directed toward the surface and can circumvent the etching reaction by increasing the incident flux of the reactive radicals. HWCVD results on patterned Si_3N_4 samples are presented in Figs. 4–7. Figs. 4 and 6 explore the effect of exposure at a constant flux of 0.3 ML/min and the effect of flux at a constant exposure of 6 ML, respectively, for growths at 975 K. Fig. 7 explores the effect of temperature at a constant flux of 0.3 ML/min and exposure of 6 ML.

With exposure, the total particle density increases and goes through a maximum that exceeds the total pore density of $6 \times 10^{10}\,cm^{-2}$ (Fig. 4a) because some pores contain more than one nanoparticle (Fig. 4b). Fig. 5 presents a SEM image of a HWCVD sample for 6 ML total exposure at 975 K. The following characteristics are the irregular particle shapes and the position of particles within the pores, which suggest that nucleation occurs randomly within a pore and that coalescence is significant during growth. At the lowest exposures, only ~30% of the pores have any particles and ultimately all the pores contain at least one particle for 15 ML total exposure (Fig. 4c). The increasing percentage (Fig. 4c) would be expected if nucleation occurs at different times (or in this case exposures) as opposed to occurring at the outset in all pores. At all exposure levels, the greatest fraction of filled pores contains one nanoparticle. The curves for multiple particles (Fig. 4b) increase at the lower exposures because multiple nucleation events are occurring in the pores; the single pore curve, which reflects the balance of the filled pores, must decrease. Ultimately, the multiple particles in a pore begin coalescing into fewer particles, and eventually form one particle.

Trends in the relative proportions of filled pores with one, two, three and four particle ensembles with exposure indicate that nanoparticles are nucleating at different times (exposures) and then growing to an observable size at longer exposures. Ultimately, the multiple particles coalesce into one particle. The 3 and 6 ML HWCVD exposures at 975 K offer insight into the question of simultaneous versus sequential particle nucleation. Pores with two particles each have equisized particles in 77% of the pores for both exposures; a 100% value would be expected for simultaneous nucleation. Pores having three particles each

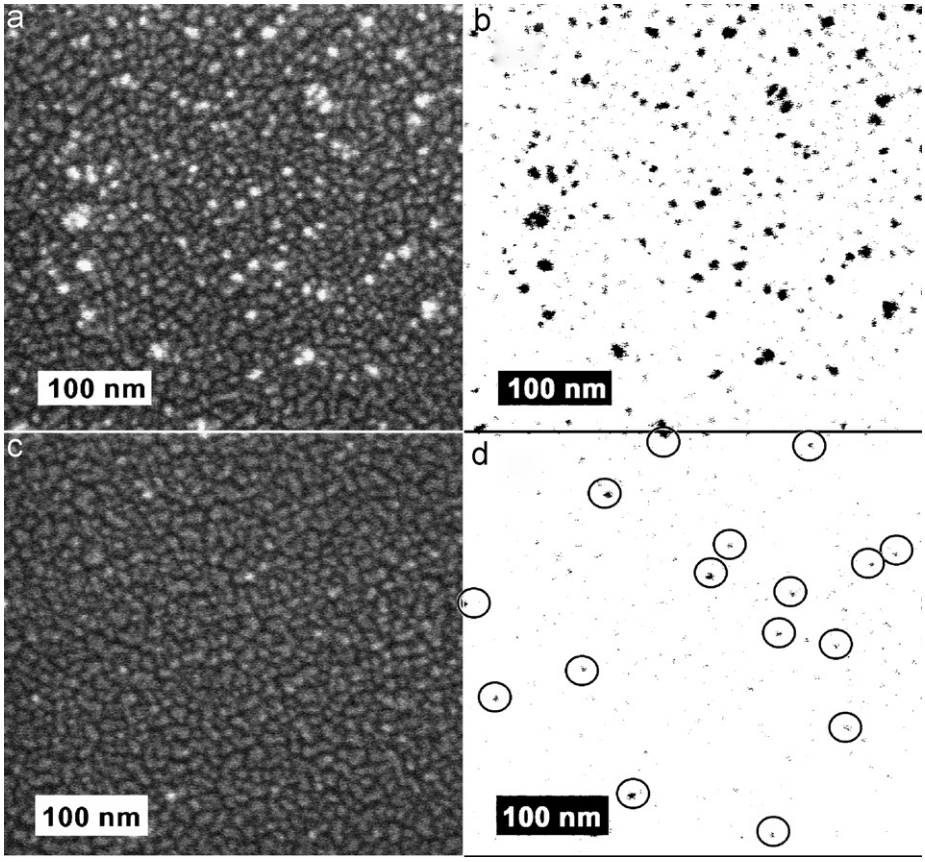

Fig. 2. SEM images of 4 min thermal CVD on extended Si_3N_4 at 975 K and a disilane pressure of 1×10^{-4} Torr. (a) The SiO_2 hard mask was removed using HF and the underlying Si_3N_4 had a 20 s exposure to the 200 W CHF_3/O_2 RIE chemistry used in processing patterned samples. The particle density is 1×10^{11} cm^{-2} and particles range in diameter from 5 to 25 nm. (b) The negative image of Part a where the particles are easily observed as black spots. (c) The SiO_2 hard mask was removed using HF without any further steps and given the same thermal CVD as Part a. The particle density is 2×10^{10} cm^{-2} and particles range in diameter from 5 to 10 nm. (d) The negative image of Part c with circles around the 16 black spots that correspond to particles greater than 5 nm in diameter.

display equisized particles in 74% of the pores for 3 ML exposure and in 42% of the pores for 6 ML exposure.

Incidence flux rate data are clustered into two regions, the low flux region at 0.09–0.4 ML/min and the high flux regions found at greater than 0.4 ML/min (Fig. 6). In the low flux regime, the fraction of filled pores remains constant at ~70% and the average particle diameter decreases as the flux is increased since increasing numbers of pores contain more than one particle. The amount of silicon deposited is constant in the 0.09–0.4 ML/min flux range at ~0.7 ng/cm^2 assuming particles are lens shaped [28]. At 0.9 ML/min flux rate, the particles completely cover the Si_3N_4 surface in 100% of the pores and grow onto the adjacent SiO_2 hard mask. This is caused by adatom accumulation overwhelming the loss processes at the perimeters of the Si_3N_4 features at the highest flux.

The fraction of filled pores and the average particle diameter decrease with increasing temperature (Fig. 7). Essentially films form in every pore at the lowest temperature, 900 K, under the flux (0.3 ML/min) and exposure (6 ML) conditions employed. The particle density goes through a maximum with temperature. The density increase to a value greater than the pore density is related to the appearance of multiple particle ensembles in the pores. The density eventually decays with increasing temperatures because etching reactions are depleting adatoms from the growth region and particles fail to nucleate or grow to an observable size during the exposure time.

4. Discussion

Selective growth of Si on arrays of Si_3N_4 surfaces defined through a sacrificial SiO_2 hard mask is qualitatively similar to the selective growth of Ge on HfO_2 defined through a sacrificial SiO_2 mask [7]. In both cases the inability of Si or Ge to accumulate on SiO_2, yet accumulate on the growth surface, enables selective deposition at the bottom of the features defined through the SiO_2 mask. The need to work above 900 K to realize facile etching of SiO_2 by Si leads to very rapid CVD reactions on Si_3N_4 and this reduces the flexibility one may have in optimizing the process through changes in temperature and Si_2H_6 partial pressure. While both CVD and HWCVD can be used to grow nanoparticles selectively as shown above, HWCVD may be the preferred method. HWCVD permits seeding of the

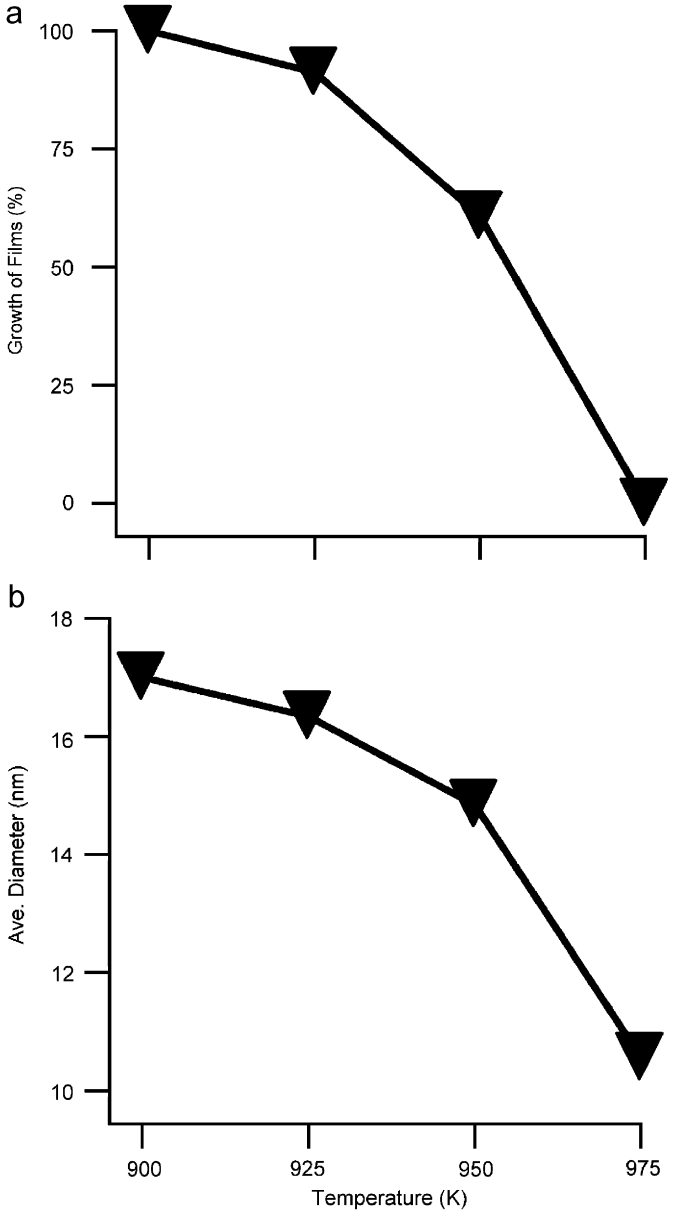

Fig. 3. (a) Fraction of pores that contain Si films versus temperature after 3 min (18,000 L) thermal CVD. *Note*: All pores contained Si in the form of nanoparticles or a continuous film. (b) Average particle diameter that considers a film to be a 17 nm particle.

nanoparticles to better control the process [7] and it permits a wide range of radical fluxes to be explored to optimize the process [23].

Selective nanoparticle deposition relies on balancing the generation and accumulation processes for the adatoms on the growth surface against the adatom loss processes. Once formed, an Si adatom can be expected to experience five possible fates in the system under consideration [15,29]: (1) diffusion on the SiO_2 or Si_3N_4 surface until it encounters and attaches to a subcritical cluster (size $< i^*$), which can lead to the adatom reentering the adatom population; (2) diffusion on the SiO_2 or Si_3N_4 surface until it encounters and attaches to a critical cluster (size $= i^*$) or

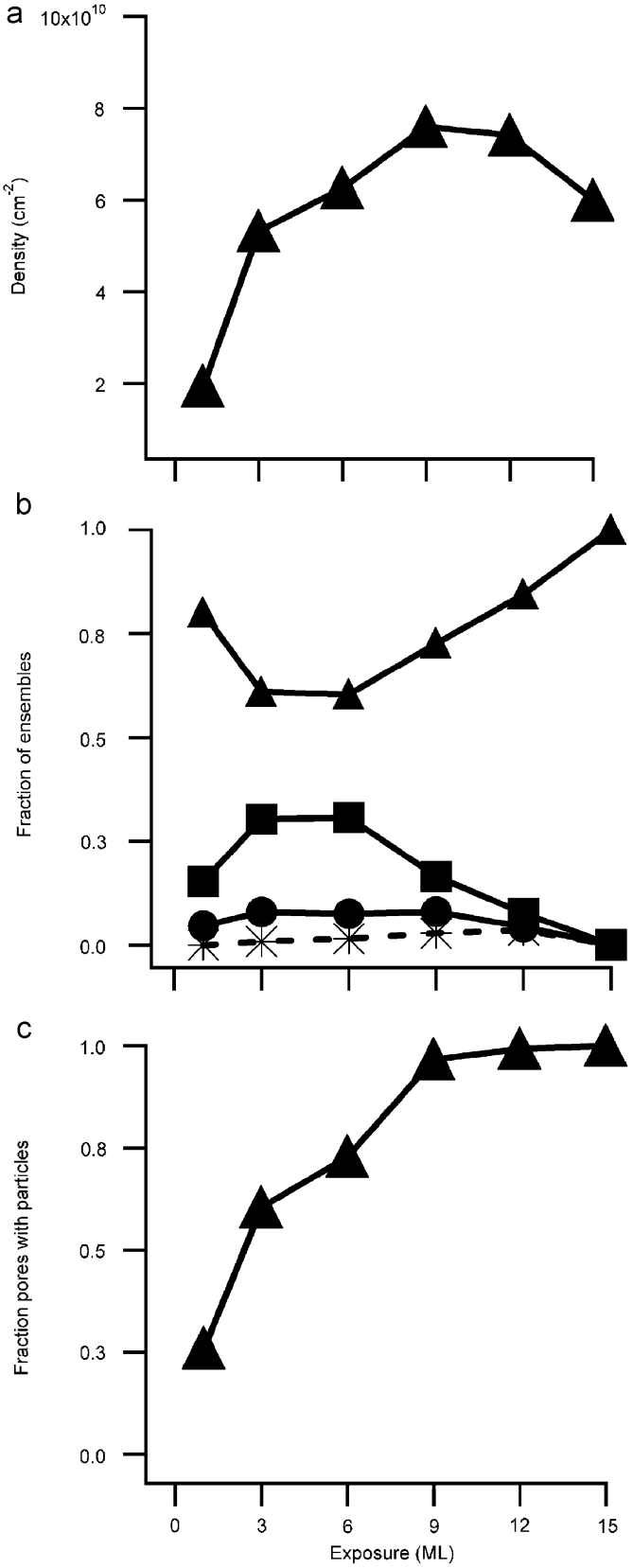

Fig. 4. Curves showing the effects of changing exposure during HWCVD at 975 K for a flux of 0.3 ML/min: (a) Si nanoparticle particle density, (b) fraction of filled pores containing ensembles consisting of a single Si particle (▲), two Si particles (■), three Si particles (●), four Si particles (✻), and (c) fraction of all available pores showing any type of particle ensemble.

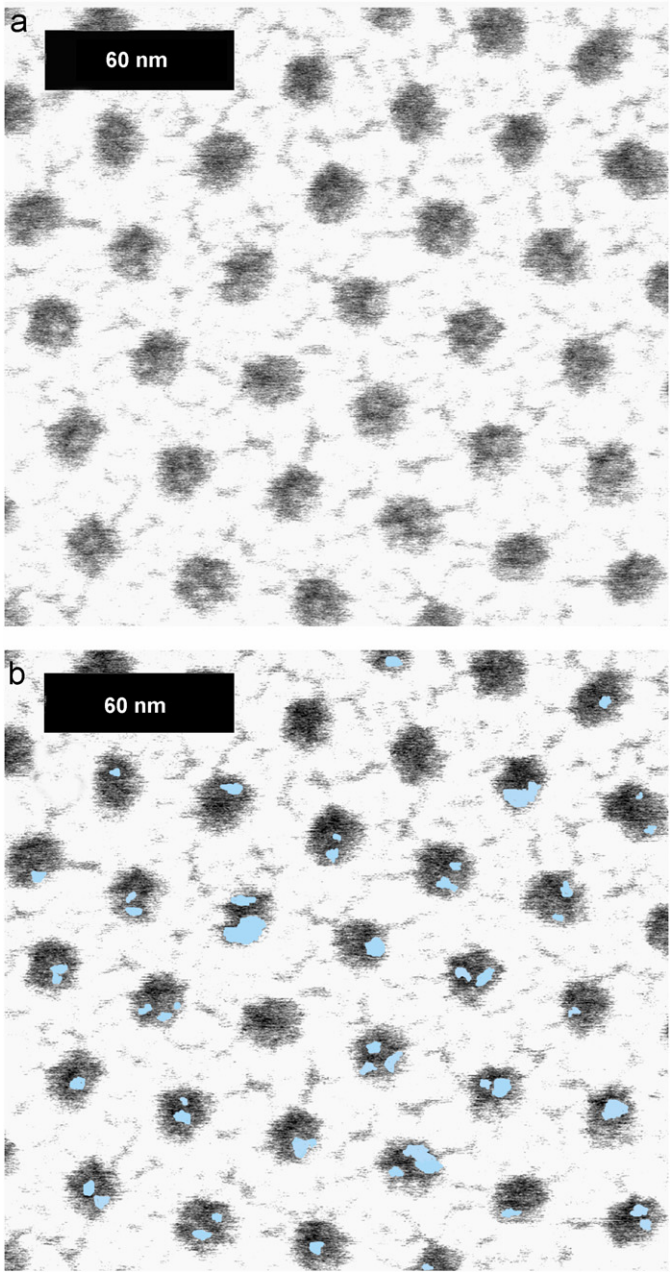

Fig. 5. (a) SEM image of a patterned Si_3N_4 HWCVD sample grown at 975 K, 0.4 ML/min flux, and 6 ML total exposure. The dark circles are the bottoms of the Si_3N_4 pores and the irregular, faint white objects in the circles are the Si nanoparticles. The continuous bright white surface surrounding the Si_3N_4 pores is the SiO_2 hard mask. (b) The image was digitally enhanced with light blue representing the nanoparticles on the dark Si_3N_4.

a stable nanoparticle (size $> i^* + 1$), which removes the adatom from the adatom population; (3) loss from the SiO_2 surface through etching reactions that produce SiO; (4) diffusion on the Si_3N_4 regions until the adatom encounters and reacts with the SiO_2 at the pore wall perimeter and is lost through etching reactions; and (5) diffusion on the SiO_2 regions until it spills over into the pores and becomes adsorbed on the Si_3N_4 regions.

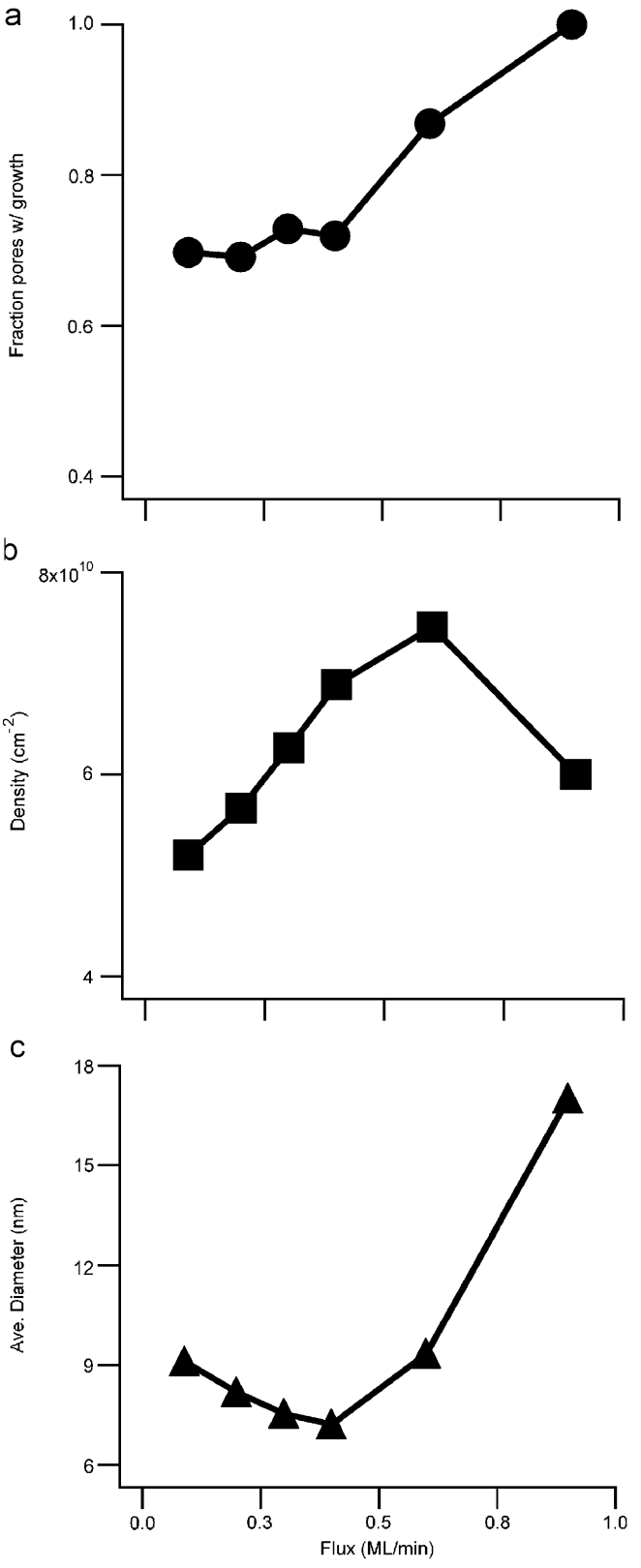

Fig. 6. Curves showing the effects of changing the flux during HWCVD at 975 K for a constant exposure of 6 ML: (a) fraction of all pores showing any particle ensemble combination, (b) overall Si nanoparticle density, and (c) average nanoparticle diameter.

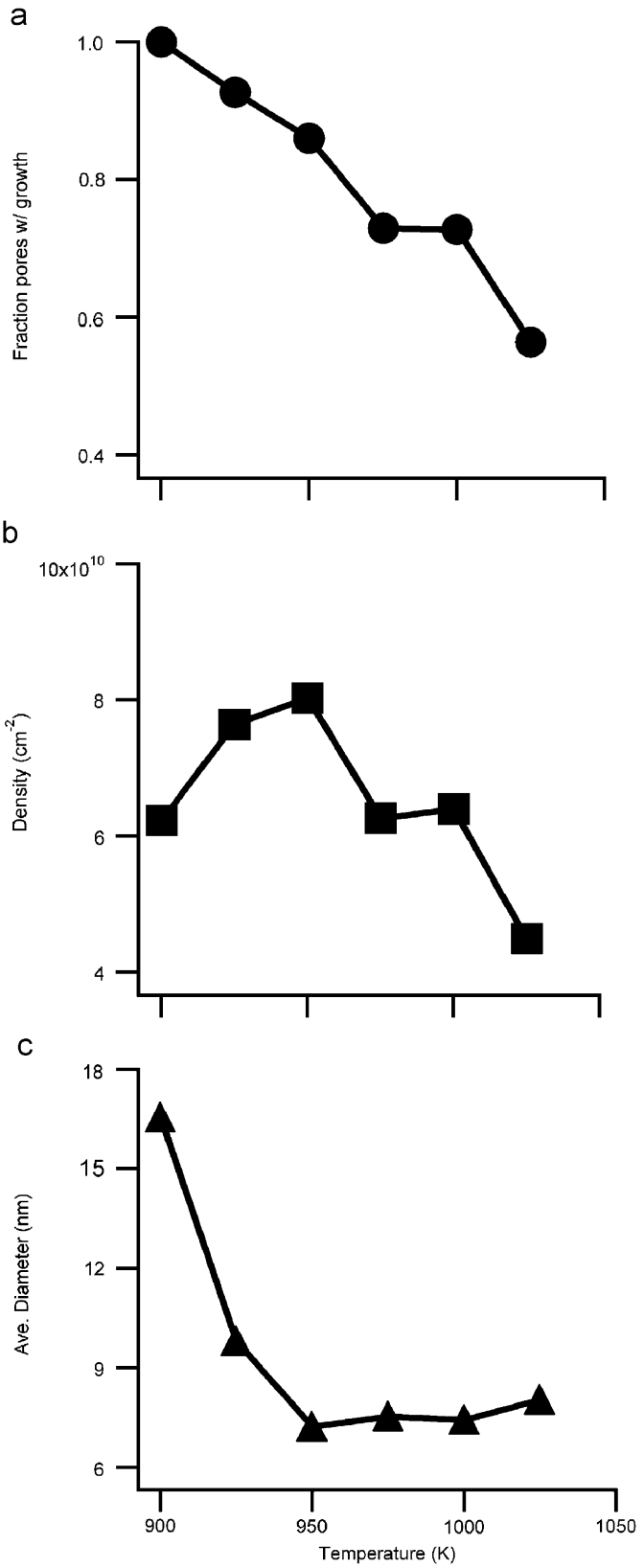

Fig. 7. Curves showing the effects of changing the temperature during HWCVD at a fixed flux of 0.3 ML/min and total exposure of 6 ML: (a) fraction of all pores showing any particle ensemble combination, (b) overall Si nanoparticle density, and (c) average nanoparticle diameter.

These processes are activated and while the absolute rates are not known, some activation energies are available permitting one to consider the relative rates and how rates change with processing conditions. The etching of SiO_2 by Si is well documented [10,30] and was expected to be sufficiently fast at 975 K that adatoms would not accumulate on the SiO_2 in CVD and HWCVD. The absence of Si nanoparticles on the SiO_2 mask seems to bear this out. Etching has an activation energy of either 0.84 [30] or 2.7 eV [10]. The activation energy of Si diffusion on Si_3N_4 may be similar in magnitude to the activation energy of Si on SiO_2 (0.47 eV) [13], which would mean that the etching reaction will increase faster than diffusion as the temperature increases. Silicon adatoms can diffuse over the relevant surface dimensions (17 nm within a pore and 23 nm between pore openings on the SiO_2 mask) very rapidly. Using the prefactor of 0.1 cm^2/s and the activation energy of 0.47 eV for Si on SiO_2 [13] to estimate a diffusion coefficient of Si on Si_3N_4, a Si adatom will have a mean squared displacement of 314 nm^2 (i.e., the area of a 20 nm pore) in ~2.2 ns. Further, given the rapid diffusion and the short distances over which the Si needs to diffuse on the SiO_2 mask, we cannot discount the possibility that some of the Si adatoms originating on the SiO_2 surface diffuse and attach to the Si_3N_4 surfaces. Such a possibility could be tested with molecular beam epitaxy where the incident flux Si atoms is known, versus in HWCVD were a mixture of radicals and stable molecules is incident on the surfaces.

In its simplest form, our model for selective growth has incident hydride radicals (on the SiO_2) leading to adatoms that do not accumulate and etch the SiO_2 surface, and incident hydride radicals (on the Si_3N_4) leading to adatoms that are contained on the Si_3N_4 surfaces at the pore bottoms until they either nucleate and/or add to a nanoparticle, or react with the SiO_2 walls and are removed by etching. Studies on amorphous surfaces have indicated that i^* is either 0 or 1 for nanoparticle growth [11,13]. Extrapolating these findings to Si on Si_3N_4, particles nucleate when an adatom diffuses on the surface until it is positioned over a site that serves as a nanoparticle anchor ($i^* = 0$) or encounters an adatom that is already at a suitable site ($i^* = 1$). The rate of nucleation has a power-law dependence on the average adatom density of $i^* + 1$ [16]. Nucleation, as manifested in multiple nanoparticles per pore and the total percentage of filled pores, increases with flux at constant temperature (Fig. 6a and b), and decreases with increasing temperature at constant flux (Fig. 7). Nucleation increases when process conditions favor a higher adatom concentration. It is not possible to estimate the steady-state coverage of adatoms on the Si_3N_4 within a pore. Given the short distances on the confined Si_3N_4 surfaces over which an Si adatom diffuses before nanoparticle nucleation and growth, and the low power-law order dependence (1 or 2) for the nucleation rate on the adatom concentration, it seems the selective growth process is dominated by etching and the concentration of adatoms within individual pores must be quite low. Beyond the

nucleation step, adatoms are required for particle growth to an observable size. The majority of silicon precursor delivered to the surface is removed through etching with SiO_2 and the low particle growth rate reflects the loss. Using HWCVD requires 15 ML silicon exposure at 975 K at a 0.3 ML/min flux to grow large enough particles within the pores to cover the exposed nitride surface. By comparison to an unpatterned nitride surface at the equivalent flux, a 2 ML exposure results in a continuous film. We conclude that the adatom removal from the nitride surface (at the pore perimeter) under the selective growth conditions is extremely quick and is the limiting factor in nucleation and particle growth.

5. Summary

We demonstrate the versatility of selective nanoparticle growth within ~17 nm pores by extending it from the Ge on HfO_2 system to the Si on Si_3N_4 system. Growth is directly on the Si_3N_4 (or HfO_2) dielectric surface, possibly simplifying future incorporation of this method into device fabrication. The silica hard mask regulates nanoparticle nucleation and growth through adatoms etching the silica and evolving as gaseous SiO. The silicon deposition rate is dependent upon the balance of the adatom removal mechanism and nanoparticle nucleation and growth reactions. Maintaining a sufficient Si flux to exceed the etching rate is key to nanoparticle growth. Nanoparticle growth decreases with increasing temperature and increases with increasing incident flux of SiH_x radicals in HWCVD.

Acknowledgments

The authors thank the Welch Foundation (Grant no. F1502), the National Science Foundation (Award ECS-0304026), and the State of Texas Advanced Research Program for funding. The authors also thank the C. Grant Willson research group for helping with polymer thin film processing and Scott Kravitz with counting and measuring pore size.

References

[1] S. Tiwari, F. Rana, H. Hanafi, A. Hartstein, E.F. Crabbe, K. Chan, Appl. Phys. Lett. 68 (1996) 1377.
[2] I. Crupi, D. Corso, S. Lombardo, C. Gerardi, G. Ammendola, G. Nicotra, C. Spinella, E. Rimini, M. Melanotte, Mater. Sci. Eng. C 23 (2003) 33.
[3] International Technology Roadmap for Semiconductors, 2005.
[4] S. Miyazaki, Y. Hamamoto, E. Yoshida, M. Ikeda, M. Hirose, Thin Solid Films 369 (2000) 55.
[5] F. Mazen, T. Baron, A.M. Papon, R. Truche, J.M. Hartmann, Appl. Surf. Sci. 214 (2003) 359.
[6] C. Basa, E.A. Irene, J. Vac. Sci. Technol. A 17 (1999) 817.
[7] S.S. Coffee, S.K. Stanley, J.G. Ekerdt, J. Vac. Sci. Technol. B 24 (2006) 1913.
[8] S.K. Stanley, S.V. Joshi, S.K. Banerjee, J.G. Ekerdt, J. Vac. Sci. Technol. A 24 (2006) 78.
[9] S.K. Stanley, S.V. Joshi, S.K. Banerjee, J.G. Ekerdt, Surf. Sci. 600 (2006) L54.
[10] W.T. Leach, J.H. Zhu, J.G. Ekerdt, J. Crystal Growth 243 (2002) 30.
[11] Q.M. Li, J.L. Krauss, S. Hersee, S.M. Han, J. Phys. Chem. C 111 (2006) 779.
[12] T. Baron, F. Martin, P. Mur, C. Wyon, M. Dupuy, J. Crystal Growth 209 (2000) 1004.
[13] M.S. Mason, J.K. Holt, H.A. Atwater, Thin Solid Films 458 (2004) 67.
[14] J.A. Venables, Phys. Rev. B 36 (1987) 4153.
[15] J.A. Venables, G.D.T. Spiller, M. Hanbucken, Rep. Prog. Phys. 47 (1984) 399.
[16] D. Kandel, Phys. Rev. Lett. 78 (1997) 499.
[17] J.A. Venables, Surf. Sci. 300 (1994) 798.
[18] Q.M. Li, B. Pattada, S.R.J. Brueck, S. Hersee, S.M. Han, J. Appl. Phys. 98 (2005) 073507.
[19] K.W. Guarini, C.T. Black, K.R. Milkove, R.L. Sandstrom, J. Vac. Sci. Technol. B 19 (2001) 2784.
[20] K.W. Guarini, C.T. Black, Y. Zhang, H. Kim, E.M. Sikorski, I.V. Babich, J. Vac. Sci. Technol. B 20 (2002) 2788.
[21] S.K. Ray, C.K. Maiti, N.B. Chakraborti, Semicond. Sci. Technol. 8 (1993) 599.
[22] T. Baron, F. Mazen, J.M. Hartmann, P. Mur, R.A. Puglisi, S. Lombardo, G. Ammendola, C. Gerardi, Solid-State Electron. 48 (2004) 1503.
[23] W.T. Leach, J.H. Zhu, J.G. Ekerdt, J. Crystal Growth 240 (2002) 415.
[24] C. Basa, Y.Z. Hu, M. Tinani, E.A. Irene, J. Vac. Sci. Technol. A 16 (1998) 3223.
[25] F. Mazen, L. Mollard, T. Baron, S. Decossas, J.M. Hartmann, Microelectron. Eng. 73–74 (2004) 632.
[26] B.A. Ferguson, C.T. Reeves, D.J. Safarik, C.B. Mullins, J. Chem. Phys. 113 (2000) 2470.
[27] S.M. Gates, Surf. Sci. 195 (1988) 307.
[28] J.H. Zhu, W.T. Leach, S.K. Stanley, J.G. Ekerdt, X.M. Yan, J. Appl. Phys. 92 (2002) 4695.
[29] H. Brune, Surf. Sci. Rep. 31 (1998) 121.
[30] D.C. Streit, F.G. Allen, J. Appl. Phys. 61 (1987) 2894.